Journal of Inflammation Research

Dovepress
Taylor & Francis Group

Open Access Full Text Article

ORIGINAL RESEARCH

The Role of Herb-Partitioned Moxibustion in the Angiogenesis of Colitis-Associated Cancer in Rats

Kunshan Li[1,2], Luyi Wu[2], Lu Zhu[1,2], Wenjia Wang[1], Yiyi Chen[1], Zhe Ma[1,2], Guangtao Zhang[3], Muen Gu[1], Hanxiao Zhang[1], Huangan Wu[1,2]

[1]Yueyang Hospital of Integrated Traditional Chinese and Western Medicine, Shanghai University of Traditional Chinese Medicine, Shanghai, People's Republic of China; [2]Shanghai Research Institute of Acupuncture and Meridian, Shanghai University of Traditional Chinese Medicine, Shanghai, People's Republic of China; [3]Seventh People's Hospital of Shanghai University of Traditional Chinese Medicine, Shanghai, People's Republic of China

Correspondence: Huangan Wu; Hanxiao Zhang, Yueyang Hospital of Integrated Traditional Chinese and Western Medicine, 110 Ganhe Road, Hongkou District, Shanghai, 200437, People's Republic of China, Email wuhuangan@126.com; zhx13750982383@163.com

Purpose: Angiogenesis in tumors is imperative to tumor growth. Our previous studies revealed that herb-partitioned moxibustion (HPM) could delay colitis-associated cancer (CAC), but the mechanism of the effects on the angiogenesis remains largely undiscovered. We aimed to investigate whether HPM delays CAC by inhibiting the angiogenesis with emergent three-dimensional (3D) imaging technologies.

Materials and Methods: The CAC model was induced by azoxymethane (AOM)/dextran sodium sulphate (DSS). The rats were randomly divided into normal, model and HPM groups. The tumorigenesis, number of tumors, and tumor diameter were observed. Immunohistochemistry or enzyme-linked immunosorbent assay (ELISA) was performed to assess the microvessel density (MVD), reactive oxygen species (ROS), hypoxia-inducible factor-1 alpha (HIF-1α), vascular endothelial growth factor A (VEGFA), vascular endothelial growth factor receptor 1 (VEGFR1), interleukin-6 (IL-6), interleukin-1 beta (IL-1β) and tumor necrosis factor-alpha (TNF-α). The three-dimensional imaging of solvent-cleared organs with superior fluorescence-preserving capability (FDISCO) tissue clearing technique was used to clear colon tissues, and the platelet endothelial cells were stained and labelled with platelet endothelial cell adhesion molecule 1 (PECAM-1). Imaris software was used to perform 3D measurement and analysis of the colonic vascular architecture.

Results: The HPM group were found decreased in the colon tumor diameter, MVD, ROS, HIF-1α, VEGFA, VEGFR1, IL-6, IL-1β, and TNF-α in colon tissues compared with those in the model group. 3D imaging revealed that the number of vessels, number of branch points, and vessel branch level in the HPM group were lower than those in the model group. The number of branch points and vessel branch level were negatively correlated with the average vessel length.

Conclusion: HPM plays a role in inhibiting CAC angiogenesis. This study may provide new evidence at the macroscopic level of vascular architecture for HPM to inhibit the progression of CAC by FDISCO tissue clearing technique for 3D imaging.

Keywords: colitis-associated cancer, herb-partitioned moxibustion, tissue clearing technique, three-dimensional visualization, vascular architecture

Introduction

Colorectal cancer (CRC) is the third most common cancer with the second highest mortality rate.[1] Colitis-associated cancer (CAC) is a subtype of CRC that can be developed from long-term inflammatory bowel disease (IBD).[2,3] CAC tends to have a worse prognosis compared with more common polyp-induced CRC.[4] How to reduce its morbidity, delay its progress and control its mortality have become hot and challenging topics for scholars to study.

Sustained angiogenesis is considered one of the fundamental features of the microenvironment in solid tumors. Vascular endothelial growth factor (VEGF) is identified as a critical factor promoting vascular permeability and angiogenesis.[5] Within tumors, hypoxic regions arise due to rapid cell proliferation and insufficient vascular supply, compelling cancer cells to adapt through the activation of Hypoxia-inducible factor-1 alpha (HIF-1α).[6] This

Received: 19 February 2025
Accepted: 8 May 2025
Published: 23 May 2025

© 2025 Li et al. This work is published and licensed by Dove Medical Press Limited. The full terms of this license are available at https://www.dovepress.com/terms.php and incorporate the Creative Commons Attribution – Non Commercial (unported, v4.0) License (http://creativecommons.org/licenses/by-nc/4.0/). By accessing the work you hereby accept the Terms. Non-commercial uses of the work are permitted without any further permission from Dove Medical Press Limited, provided the work is properly attributed. For permission for commercial use of this work, please see paragraphs 4.2 and 5 of our Terms (https://www.dovepress.com/terms.php).

adaptation promotes angiogenesis by upregulating VEGF.[7] The response of HIF-1α to hypoxia is related to the production of reactive oxygen species (ROS) induced by hypoxia.[8,9] Angiogenesis and VEGF signaling might be an important link between inflammation and tumor development in CAC. Patients with CAC show activated VEGFR on intestinal epithelial cells, and blockade of VEGF function suppressed tumor development, inhibited tumor angiogenesis, and blocked tumor cell proliferation.[10] HIF-1α and VEGFA expressions were increased in CAC mice.[11] Studies have suggested that intracellular ROS accumulation increased the HIF-1α levels in CRC cells, and the ROS inhibitor can reverse elevation of HIF1-α.[12] Additionally, ROS can activate HIF-1α by inhibiting prolyl hydroxylases.[13]

In recent years, tissue transparency technology has the advantage of high imaging depth, which has been used to study vascular structure at the macro level of tissues and organs. This technology can comprehensively and accurately reflect subtle changes in vascular architecture under physiological and pathological conditions in tissues and organs, enabling researchers to enter a new field of vessel imaging.[14] However, no studies have been identified regarding three-dimensional (3D) vascular imaging of CAC. Current studies on vascular aspects of CAC models predominantly focus on indirect assessment of angiogenesis by detecting the expression of angiogenesis-related factors, such as VEGF, microvessel density (MVD), HIF-1α, matrix metalloproteinase 10 (MMP 10), angiogenin 4 (Ang 4), or cyclooxygenase 2 (COX2).[15–17] Clinical studies on 3D vascular reconstruction in CRC predominantly utilize CT-based methodologies.[18–21]

Herb-partitioned moxibustion (HPM), as a type of moxibustion, can not only provide warm stimulation to acupoints, but also promote the transdermal absorption of herbs to enhance therapeutic effects. Study has found that HPM were one of the commonly used moxibustion methods for treating cancer-related diseases.[22] HPM has been used for many years by our research team to treat IBD diseases.[23–27] The traditional Chinese medicine ingredients in herbal cakes gently warm and tonify kidney yang, promote blood circulation and remove blood stasis, promote Qi and relieve pain, which can improve the symptoms of CAC patients. Current evidence indicates that in the early phase of CRC moxibustion combined with acupuncture, which is used as an effective adjuvant to conventional interventions (surgical resection, radiotherapy, and chemotherapy), can improve treatment efficacy, reduce adverse reactions, and promote recovery in patients; In the late phase of CRC, moxibustion combined with acupuncture can improve patients' symptoms and their quality of life, and prolong their survival time.[28,29] Studies have shown that HPM can delay the progression of colon tumors in CAC rats, and our previous research revealed that HPM can reduce the expression of VEGF in CAC rats.[30–33] However, there is limited understanding of angiogenesis in CAC, and even less is known regarding the effects of HPM therapy on vasculature of CAC.

In this study, we first investigated whether HPM inhibited the expression of angiogenesis-related markers (MVD, ROS, HIF-1α, VEGFA, and VEGFR1) and pro-inflammatory cytokines (interleukin-6 [IL-6], interleukin-1 beta [IL-1β] and tumor necrosis factor-alpha [TNF-α]). On the basis of confirming the effectiveness of HPM on angiogenesis, we explored the change of tumor vascular structure in 3D by three-dimensional imaging of solvent-cleared organs with superior fluorescence-preserving capability (FDISCO) and platelet endothelial cell adhesion molecule 1 (PECAM-1) staining. We found that HPM played a role in inhibiting the formation of branch blood vessels. Currently, there are few studies observing the effect of HPM on angiogenesis in CAC. This study may provide laboratory evidence to understand how HPM delays the progression of CAC.

Materials and Methods

Animals

Thirty-one male Sprague-Dawley rats with body weights of 100±20 g were provided by Shanghai Slack Laboratory Animal Limited Company. The rats were maintained at 18–22 °C with 50–70% humidity under a 12-h light/dark cycle environment. All experiments were conducted in accordance with the requirements of the Animal Ethics Committee of Shanghai University of Traditional Chinese Medicine (ethical approval number: PZSHUTCM2306050013). After one week of adaptive feeding, the rats were randomly divided into eleven normal rats and twenty model rats.

Animal Model

CAC develops from long-term inflammation of IBD. The chemically induced models are the most commonly used method for CAC.[34] Chemically inducible CAC models typically begin with the administration of a carcinogenic compound, such as azoxymethane (AOM). AOM administration seems to be important to the CAC induction method, since the carcinogenic effect is achieved with just one administration.[34] Long-term chronic inflammation is induced by repeated cyclic stimulation of dextran sodium sulphate (DSS), resembling ulcerative colitis in humans.[35] The dosage of AOM and DSS is based on continuous exploration by previous studies of other researchers and our pilot research. Tajasuwan L and other researchers used 15 mg/(kg·bw) of AOM to create the CAC model in rat.[36–38] The concentration of the DSS was based on our previous research.[31] Twenty model rats were received 2 mg/mL AOM (SigmaSigma-Aldrich, Saint Louis, USA) at a concentration of 15 mg/(kg·bw) by intraperitoneal injection. One week after the AOM injection, the treatment was followed by three cycles of inflammatory stimulation by drinking 4–3% DSS (MP Biomedicals, Illkirch, France). Each of the three DSS cycles lasted for 4 days and was followed by 17 days of regular water (Figure 1A). Eleven normal rats in the normal group were given regular water. Following model establishment, two animals were randomly selected from the normal rats and model rats to determine whether the model was successfully established by histopathological assessment of tumorigenesis.

Grouping and Intervention

Following successful model induction, the eighteen model rats were randomly allocated into a model group and an HPM group, with nine rats in each group. Bilateral Tianshu (ST25) and Qihai (CV6) acupoints were selected for HPM treatment in the HPM group. Tianshu (ST 25) is Front-Mu point of the large intestine, and Front-Mu points are often used to treat Fu-organ diseases. Therefore, Tianshu (ST 25) can regulate the intestines. Qihai (CV6) is the place where the innate Yuan Qi gathers. It can tonify the Yuan Qi, regulate Qi movement. Qihai (CV 6) is located in the lower abdomen near the intestines, which also has the effect of treating intestine disease. Thus, Tianshu (ST25) and Qihai (CV6) points

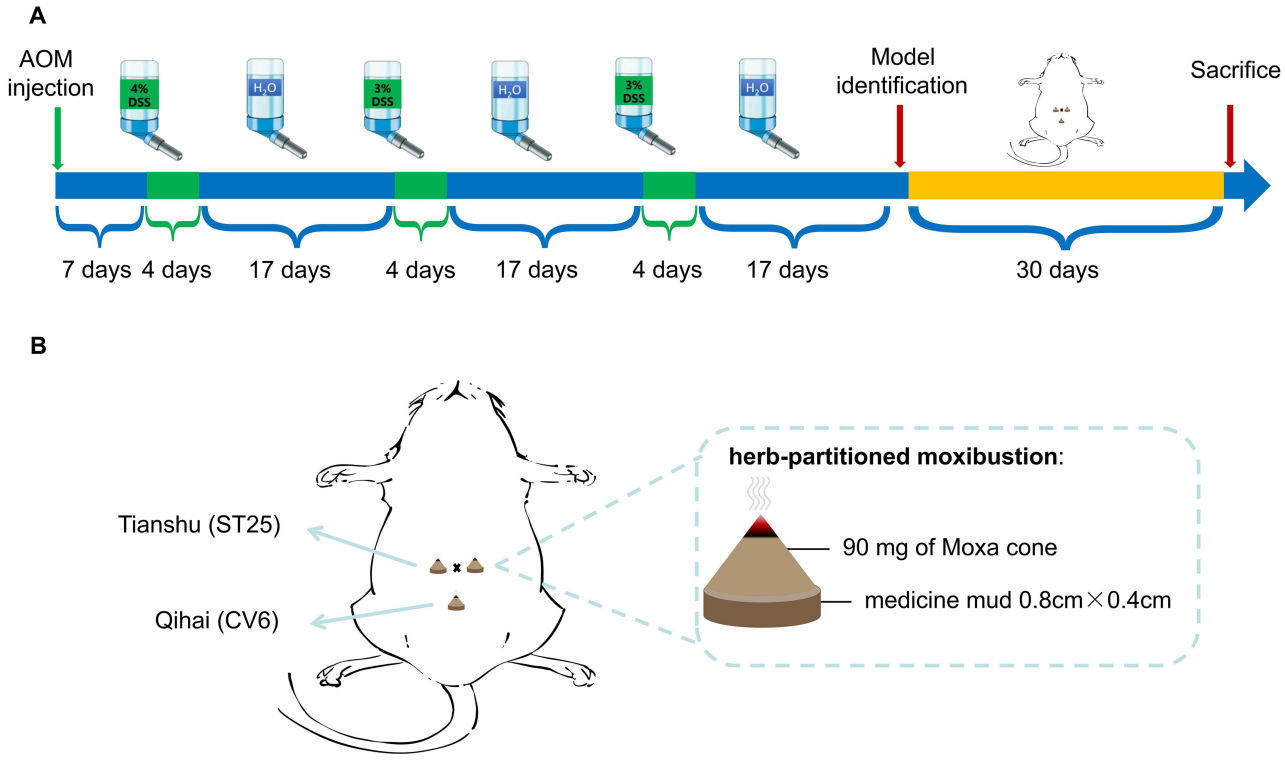

Figure 1 The flow chart of this experiment. (**A**) Schematic diagram of the AOM/DSS-induced CAC model and interventions. (**B**) Illustration of herb-partitioned moxibustion.

Abbreviations: AOM, azoxymethane; DSS, dextran sodium sulphate; CAC, colitis-associated cancer.

https://doi.org/10.2147/JIR.S518214

have the effects of inspiring lower Jiao Yang Qi, raising the clear and lowering the turbid, tonifying the deficient. Tianshu (ST 25) and Qihai (CV 6), recognized as core therapeutic acupoints in the management of IBD, a chronic condition with established progression to CAC.[23,25,39] Studies have found that HPM could relieve the clinical symptoms of patients with IBD and reduce the expression TNF-α, tumor necrosis factor receptor 1 (TNFR1), interleukin-2 (IL-2), lipopolysaccharide (LPS), or anti-toll-like receptors 4 (TLR4) in intestinal mucosa.[23,25,39] In addition, studies have found that HPM at Tianshu (ST25) and Qihai (CV6) can inhibit colon tumor proliferation in CAC rats, promote purinergic ligand-gated ion channel 7 receptor (P2X7R) and axis inhibitor (Axin) protein expression in colon tissue, meanwhile inhibit signal transducers and activators of transcription 3 (STAT3), nuclear factor kappa B p65 (NF-κB p65), proliferating cell nuclear antigen (PCNA), histone lysine demethylase 4D (KDM4D) and VEGF protein expression.[32,33]

The Tianshu (ST25) acupoint is located 5 mm on both sides of the rat navel, which is at the intersection of the upper 2/3 and lower 1/3 of the line connecting the xiphoid process and the upper edge of the pubic symphysis on the midline of the abdomen; Qihai (CV6) acupoint is located on the median line of the rat's abdomen, 12.5 mm below the rat navel.[21–23] The herbal powder formula used was as follows: Fuzi (radix Aconiti carmichaelii; 10 g, Sichuan, China), Rougui (Cinnamomum cassia Presl; 2 g, Guangxi, China), Danshen (radix Salviae miltiorrhizae; 3 g, Anhui, China), Honghua (Carthamus tinctorius L.; 3 g, Henan, China), and Muxiang (Saussurea costus; 2 g, Yunnan, China). The herb powder and an appropriate amount of yellow wine were mixed to make an herb mud. The herb mud was pressed into an herb cake with a diameter of 0.8 cm and a thickness of 0.4 cm using a mold and placed on the Tianshu (ST25) and Qihai (CV6) acupoints. Approximately 90 mg of Moxa cones were placed on the herb cakes (Figure 1B). Two moxa cones were ignited and allowed to burn at each acupoint, once daily for a total of 30 times. The rats in the normal and model groups only received the same amount of fixation as those in the HPM group without other interventions.

Sample Collection

After 30 days of intervention, the nine rats in each group were fasted for 24 h and anesthetized with 2% sodium pentobarbital [dose 40–50 mg/(kg·bw)]. One rat in each group was randomly selected for tissue transparency pretreatment: Thoracotomy was performed for cardiac exposure following deeply anesthesia. Perfusion of phosphate-buffered saline (PBS, 1×) was conducted via the left atrial chamber until achieving complete hepatic blanching. The left atrium was slowly injected with 4% paraformaldehyde solution until the tail became stiff. The abdominal cavity was subsequently cut open, and 1 cm of the colon was cut. The colon was fixed in 4% paraformaldehyde for 3 days and then placed in PBS solution in a refrigerator at 4 °C for tissue transparency. After the necks of the remaining 24 rats were severed, and the colon from the pubic symphysis to the ileocecal area was removed. The number and length of colon tumors were measured. For hematoxylin-eosin (HE) staining and immunohistochemistry, an approximate 1 cm length of colon tissue (including the tumor) was fixed with 4% paraformaldehyde. For the enzyme-linked immunosorbent assay (ELISA), the colon tissues were cut into pieces, stored and prepared for use in a −80 °C freezer.

HE

HE staining was used to observe the histopathology of the colon tissue of the rats. The slices were routinely dewaxed. The sections were stained with hematoxylin for 2 min, rinsed with tap water for 10 min, differentiated with 1% hydrochloric acid alcohol for 2 s, rinsed with tap water for 5 min, and stained with eosin for 2 min. The sections were dehydrated in alcohol solutions (70%, 80%, 90% and 100%) separately for 2 s, and xylene I and II were soaked respectively for 15 min to make the sections transparent. Neutral gum was used for sealing.

ELISA

ELISA was used to detect the contents of ROS, IL-6, IL-1β and TNF-α (Mlbio, Shanghai, China) in the colon tissues of the rats. The proper amount of normal saline was added, then the tissue was mashed. Three thousand revolutions per min centrifuge for 10 min to remove the supernatant. According to the manufacturer's protocol, the corresponding standard and sample were added to the standard well and sample well, respectively. The antibody, substrate and termination solution were added successively into the standard well and sample well, and the optical density (OD) value of each well was subsequently determined.

Immunohistochemistry

The protein expression of cluster of differentiation 34 antigen (CD34), HIF-1α, VEGFA and VEGFR1 in the colon tissues was detected by immunohistochemistry. The paraffin-embedded sections were deparaffinized before heating with citrate buffer for high-temperature repair. The sections were incubated with 3% hydrogen peroxide at room temperature for 25 min, then washed with PBS. The tissue was uniformly covered with 3% BSA and incubated at room temperature for 30 min. Furthermore, each section was sequentially incubated with anti-CD34 (1:500, Abcam, Cambridgeshire, UK), anti-HIF-1α (1:100, Thermo Fisher Scientific, Waltham, USA), anti-VEGFA (1:200, Abcam, Cambridgeshire, UK), and anti-VEGFR1 (1:250, Abcam, Cambridgeshire, UK)] at 4 °C overnight, and washed with PBS. The sections were incubated with secondary antibody at room temperature for 50 min and then developed with 3, 3′-Diaminobenzidine (DAB) solution for 5 min. Finally, the sections were counterstained with hematoxylin for 3 min, and dehydrated in graded ethanol. Three fields of each section were randomly photographed, and the images were imported into Image-PlusPro 6.0 software to calculate the positive target area and integrated optical density (IOD) of each image. The average optical density (AOD) is equal to IOD ÷ positive target area.

MVD

To calculate the MVD, areas with relatively high densities of CD34-positive cells and cell clusters were classified as "hot spots" relative to neighboring areas. Five fields with the highest number of microvessels or vascular "hot spots" were identified at low magnification (× 100). The number of microvessels or vascular in each "hot spots" field of view was manually calculated under medium magnification (× 200), and the average value was regarded as the value of the MVD.

FDISCO

The FDISCO process mainly includes perfusion, methanol-based bleaching, immunofluorescence, and tissue transparency. The perfusion operation process is detailed in the Sample Collection section. The methanol-based bleaching procedures were as follows: The colon tissues were shaken in PBS at room temperature for 30 min and the process was repeated 3 times. Subsequently, the tissues were dehydrated in graded methanol (20%, 40%, 60%, 80%, and 100%) with immersion in each concentration for 2 h. The tissues were then washed with 100% methanol for 1 h and then cooled at 4 °C. The tissues were incubated overnight in 66% dichloromethane diluted with 33% methanol and under constant agitation at room temperature. The specimens were washed twice with 100% methanol at room temperature and then cooled at 4 °C. Depigmentation was achieved via overnight at 4°C in freshly prepared 5% hydrogen peroxide (30% H_2O_2 : methanol = 1:5). Rehydration was performed through immersion in graded methanol (80%, 60%, 40%, and 20%) with each concentration for 1 h and then the tissues washed in PBS at room temperature for 1 h. Final procedure involved the samples were washed for 1 h twice in PTx.2 (each 1L of PTx.2 consisted of 100 mL of 10×PBS and 2 mL of TritonX-100) at room temperature.

The immunofluorescence procedures were as follows: The tissues were incubated in permeabilization solution (each 500 mL permeabilization solution consisted of 400 mL PTx.2, 11.5 g glycine, and 100 mL dimethyl sulfoxide) at 37 °C for 1 day and then in blocking solution (each 50 mL blocking solution consisted of 42 mL PTx.2, 3 mL donkey serum, 5 mL dimethyl sulfoxide) at 37 °C for 1 day. The anti-PECAM-1 (1:100, R&D Systems, Minnesota, USA) was incubated in PTwH (each 1 L PTwH consisted of 100 mL of 10 × PBS, 2 mL of Tween-20, 1 mL of 10 mg/mL heparin stock solution)/5% dimethyl sulfoxide/3% donkey serum at 37 °C for 3 days. The tissues were washed 4–5 times in PTwH for 2 days. The secondary antibody was incubated in PTwH/3% donkey serum at 37 °C for 3 days. The tissues were washed 4–5 times in PTwH for 2 days.

The specific transparency procedures were as follows: The samples were dehydrated in graded methanol (20%, 40%, 60%, 80%, and 100%) with each concentration for 1 h at room temperature. The specimens were then incubated in 66% dichloromethane diluted with 33% methanol under constant agitation at room temperature for 3 h. The tissues were incubated in 100% dichloromethane for 15 min and washed away the methanol for twice. The tissues were then incubated in dibenzyl ether. The tube should be almost completely filled with dibenzyl ether to prevent air from oxidizing the sample. Before imaging, the tube was inverted several times to mix the solution.

Vascular Imaging and Vascular Architecture Analysis

The tissues were imaged using an LS18 light-sheet microscope. The original data obtained by the microscope were converted using LS18 ImageCombine software and then processed in Imaris 3D image processing software. The imaging parameters were X direction by 2 μm, Y direction by 2 μm, and Z direction by 5μm, with z-stack of 2.5μm. Semi automatic reconstruction of the vascular structure was performed through surface and filament trace function in Imaris. To analyze the blood architecture quantitatively, 5 cubes with no duplication were randomly cropped when the filament trace function was performed. The reconstructed colonic blood vessel measurements were automatically generated for analysis and comparison after the relevant operations were completed.

Statistical Analysis

Statistical analysis was performed by Statistical Product and Service Solutions (SPSS, version 26.0) software. If the measurement data conformed to a normal distribution, they were expressed as the mean ± standard deviation. One-way analysis of variance (One-way ANOVA) was used for comparisons among groups, with least significant difference (LSD) or Tamhane's post-hoc test (LSD method for homogeneity of variance, Tamhane's method for heterogeneity of variance). If the data did do not conform to a normal distribution, they were expressed as the median (quartile). The Kruskal–Wallis test was used for comparisons among groups, and *p*-values were adjusted for multiple testing using the Bonferroni correction. Count data were presented as numbers, and the Fisher's exact test was used for comparison between groups. Spearman correlation analysis was calculated for the comparison between the number of branch points or vessel branch level data and the average vessel length data. $P_{adj} < 0.05$ were considered as significant.

Results

CAC Model was Successfully Induced by AOM/DSS

The successful establishment of CAC model was confirmed through macroscopic tissue observation and histopathological examination. The colons of the model rats formed tumors, with neoplastic lesions occupying approximately two-thirds of the distal colonic segment (Figure 2A). Histopathological evaluation via HE staining confirmed the formation of colon adenocarcinoma (Figure 2B).

HPM Ameliorated the AOM/DSS-Induced CAC in Rats

A reduction trend was observed in both overall tumorigenesis and the number of colonic tumors following HPM administration (Figure 3A–C). The colorectal tumor diameter in the HPM group was smaller than those in the model group ($P < 0.05$; Figure 3D). Histopathology revealed distinct morphological differences among groups (Figure 3E). The normal group displayed characteristic physiological architecture: clearly demarcated mucosal layers, structurally intact epithelium, and regularly aligned glandular units. The model group exhibited characteristic atypical hyperplasia: marked mucosal hyperplasia accompanied with substantial glandular atrophy, disorganized cellular stratification and significant cellular pleomorphism, nuclear hyperchromasia, increased nuclear-cytoplasmic ratio, interstitial congestion and edema, some glandular cavities highly dilated, and "co-wall" or "back-to-back" glands. HPM intervention attenuated these pathological changes, including relatively preserved glandular alignment, partial goblet cell disappearance, attenuated nuclear hyperchromasia, and reduced glanduloepithelial dysplasia.

HPM Attenuated Intestinal Angiogenesis and Inflammation in CAC Rats

To investigate whether HPM inhibited the expression of angiogenesis- and inflammation-related cytokine in CAC Rats, we further analyzed the expression levels of MVD, ROS, HIF-1α, VEGFA, VEGFR1, IL-6, IL-1β and TNF-α. The VEGF/VEGFR axis is indispensable in the process of angiogenesis in CAC. VEGF is expressed after the activation of HIF-1α in response to hypoxia and metabolic stress. VEGF also is mediated by IL-6. IL-1β and TNF-α exhibit increased synergistically with VEGF in CAC. Through immunohistochemistry (Figure 4A, C, D and E) and ELISA (Figure 4B), we found that the MVD, the contents of ROS, IL-6, IL-1β, TNF-α, and the expression levels of HIF-1α, VEGFA, VEGFR1 proteins in the model group were distinctly increased compared to the normal group ($P < 0.001$, $P < 0.001$, $P < 0.001$, $P < 0.001$, $P < 0.001$, $P < 0.001$, $P < 0.01$, $P < 0.001$),

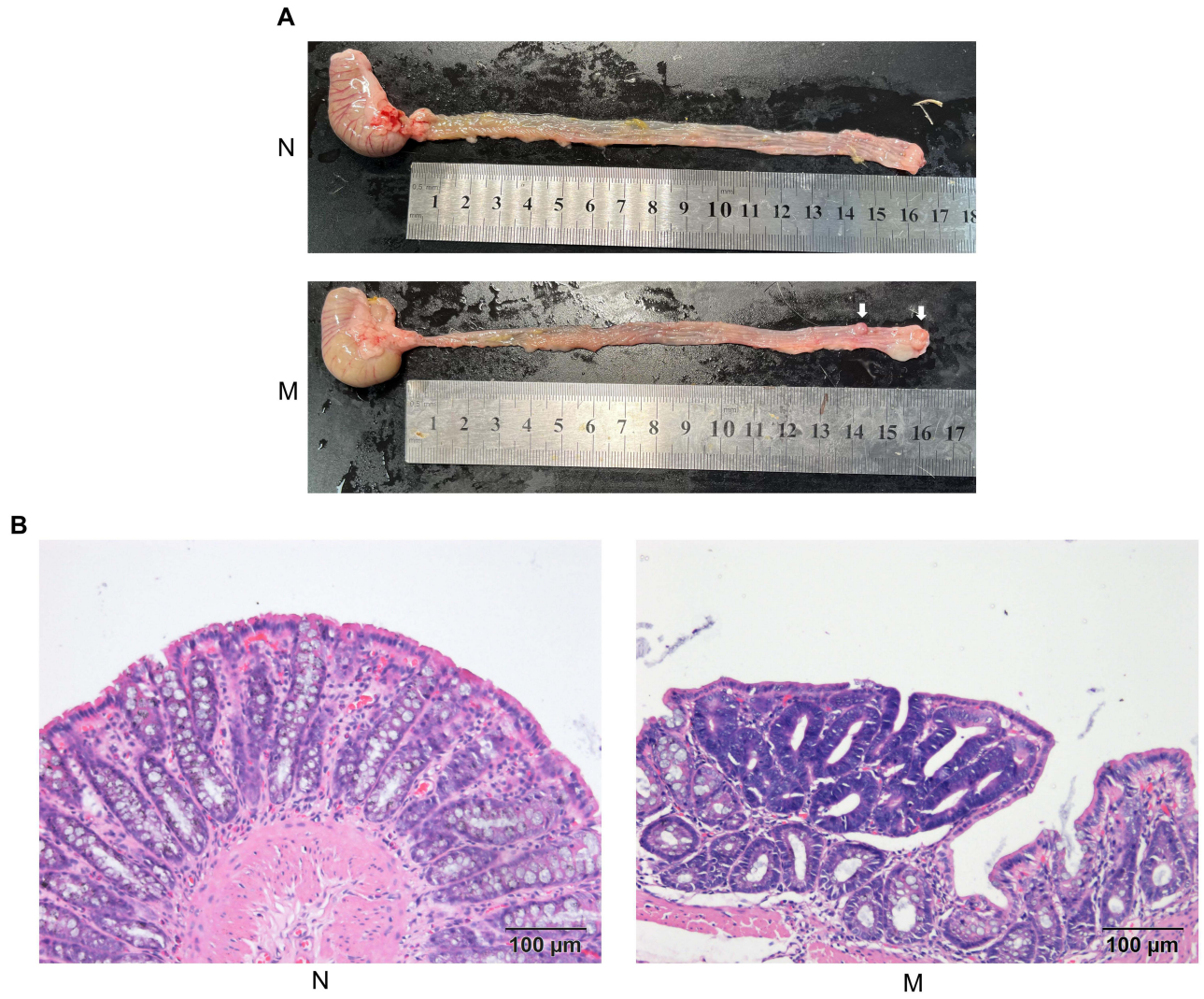

Figure 2 CAC model was successfully induced by AOM/DSS. (**A**) Representative images of the colonic tissue at model validation. (**B**) Representative images of HE staining in the normal and model rats. Scale bar: 100 μm.
Abbreviations: N, normal rat; M, model rat; CAC, colitis-associated cancer; AOM, azoxymethane; DSS, dextran sodium sulphate; HE, hematoxylin-eosin.

and significant reductions in MVD, the contents of ROS, IL-6, IL-1β, TNF-α, and the expression levels of HIF-1α, VEGFA, and VEGFR1 proteins were observed in the HPM group compared to the model group ($P < 0.05$, $P < 0.001$, $P < 0.01$, $P < 0.001$, $P < 0.001$, $P < 0.001$, $P < 0.01$, $P < 0.001$). These results indicated that HPM may attenuate intestinal angiogenesis and inflammation in CAC rats.

Colon Tissues were Rendered Visually Transparent After Clearing with FDISCO

To explore the 3D vascular structure of the tumors, we dissected part of the normal tissue in the normal group and the tumor tissues in the model and HPM groups. The tissues were cleared by FDISCO for 3D imaging (Figure 5).

3D Structure of Colon Tumors

Through the original signal presentation of the colon tissue, it could be observed that there was larger tumor tissue in the colon lumen of the model group, and relatively smaller tumor tissue in the colon lumen of the HPM group. After surface signal processing in Imaris 3D image software, tumors were more visible (Figure 6).

https://doi.org/10.2147/JIR.S518214

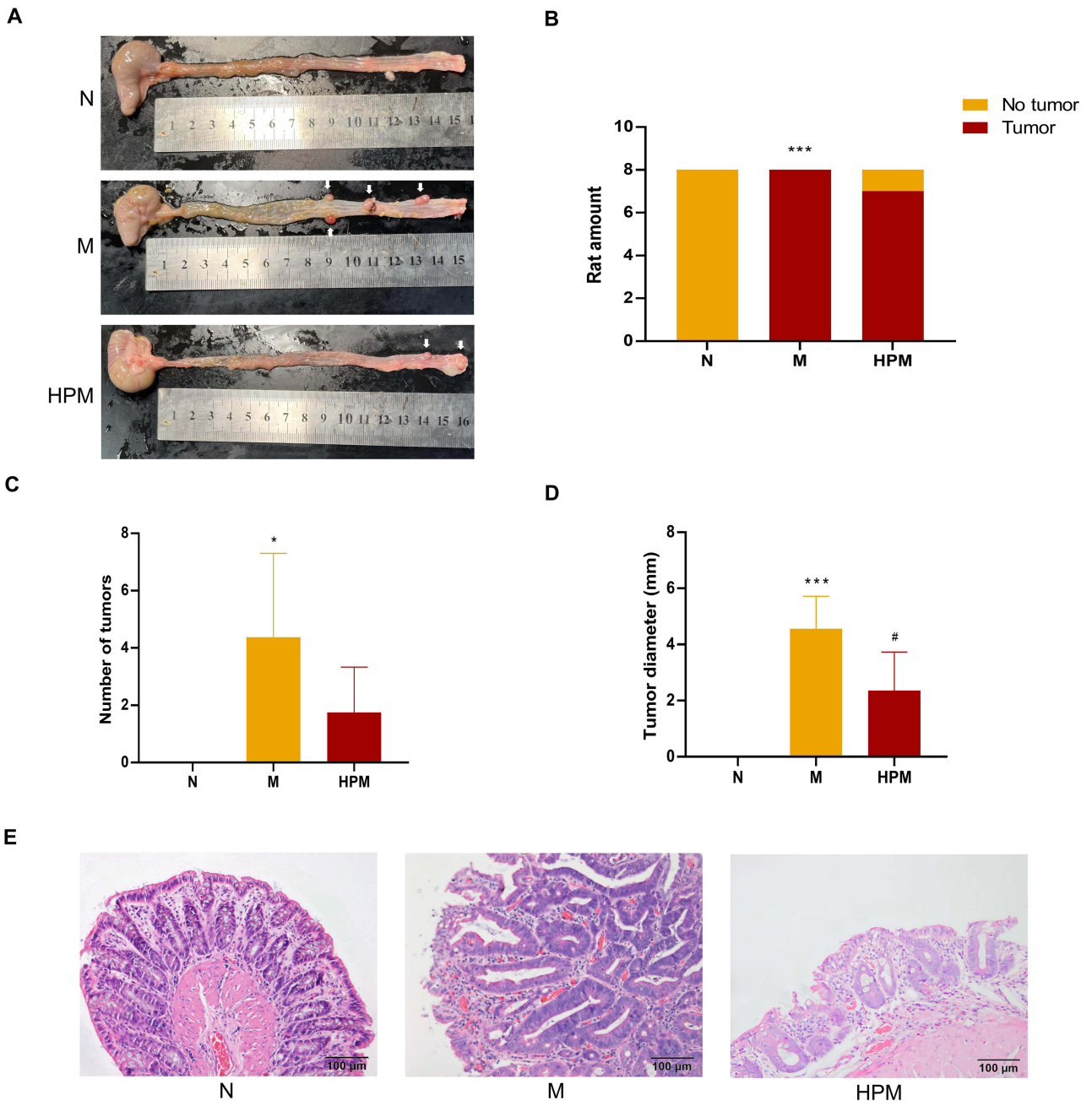

Figure 3 HPM ameliorated the AOM/DSS-induced CAC in rats. (**A**) Representative images of the colonic tissue at sacrifice. (**B**) Tumorigenesis in the colons of the normal, model and herb-partitioned moxibustion groups. (**C**) Number of tumors in the colons of the normal group, model and herb-partitioned moxibustion groups. (**D**) Tumor diameter in the colons of the normal group, model and herb-partitioned moxibustion groups. (**E**) HE staining in the colons. Scale bar: 100 μm. Statistical significance was determined by Fisher's exact test or One-way ANOVA (n=8), $^{*}P < 0.05$, $^{***}P < 0.001$ (M vs N); $^{\#}P < 0.05$ (HPM vs M).

Abbreviations: N, normal group; M, model group; HPM, herb-partitioned moxibustion group; AOM, azoxymethane; DSS, dextran sodium sulphate; CAC, colitis-associated cancer; HE, hematoxylin-eosin; One-way ANOVA, one-way analysis of variance.

HPM Recovered 3D Vascular Architecture in CAC Rats

To explore the 3D vascular architecture, we calculated the spatial parameters of vessels, including number of vessels, average vessel diameter, average vessel length, number of branch points, and vessel branch level. Compared with the normal group, the model group exhibited an increased number of colonic vascular branches with disorganized morphology and a reticular distribution pattern. In contrast to the model group, the HPM group showed a reduction in branched vessels, which were predominantly arranged in a linear configuration (Figure 7A). The number of blood vessels, number

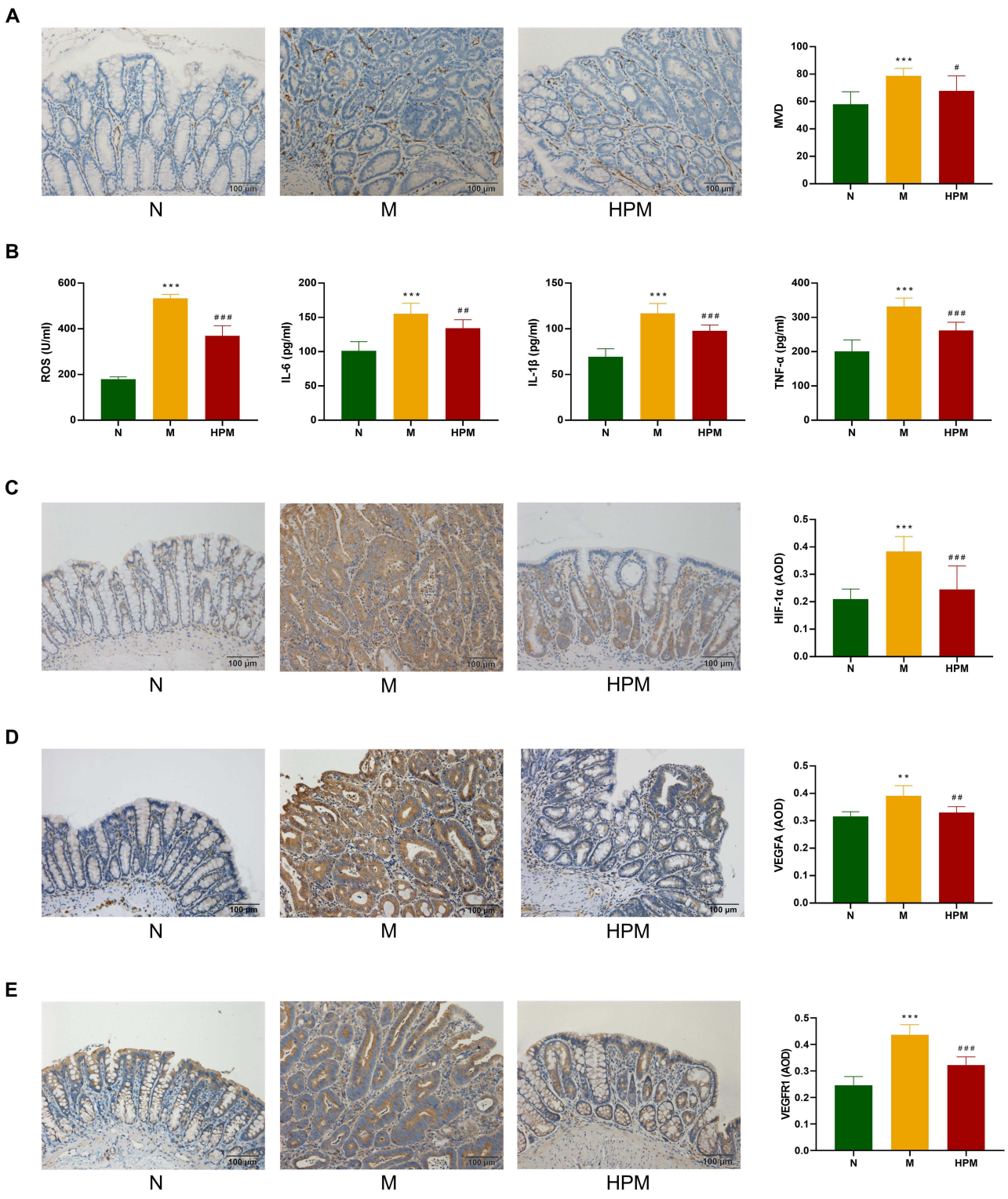

Figure 4 HPM Attenuated Intestinal Angiogenesis and Inflammation in CAC Rats. (**A**) Comparison of MVD in the colons. (**B**) Contents of ROS, IL-6, IL-1β and TNF-α in the colons. (**C**–**E**) Immunohistochemical observation of the HIF-1α, VEGFA, VEGFR1 protein expression. Scale bar: 100 μm. Statistical significance was determined by One-way ANOVA (n=8), $^{**}P < 0.01$, $^{***}P < 0.001$ (M vs N); $^{\#}P < 0.05$, $^{\#\#}P < 0.01$, $^{\#\#\#}P < 0.001$ (HPM vs M).

Abbreviations: N, normal group; M, model group; HPM, herb-partitioned moxibustion group; MVD, microvessel density; ROS, reactive oxygen species; IL-6, interleukin-6; IL-1β, interleukin-1 beta; TNF-α, tumor necrosis factor-alpha; HIF-1α, hypoxia-inducible factor-1 alpha; VEGFA, vascular endothelial growth factor A; VEGFR1, vascular endothelial growth factor receptor 1; One-way ANOVA, one-way analysis of variance; AOD, average optical density.

https://doi.org/10.2147/JIR.S518214

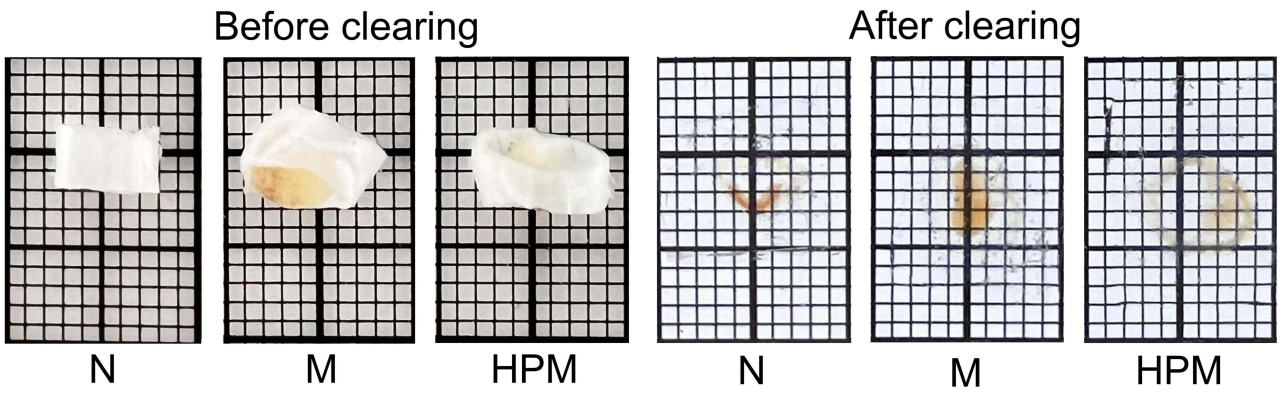

Figure 5 Brightfield images of colon tissues before and after tissue clearing.
Abbreviations: N, normal group; M, model group; HPM, herb-partitioned moxibustion group.

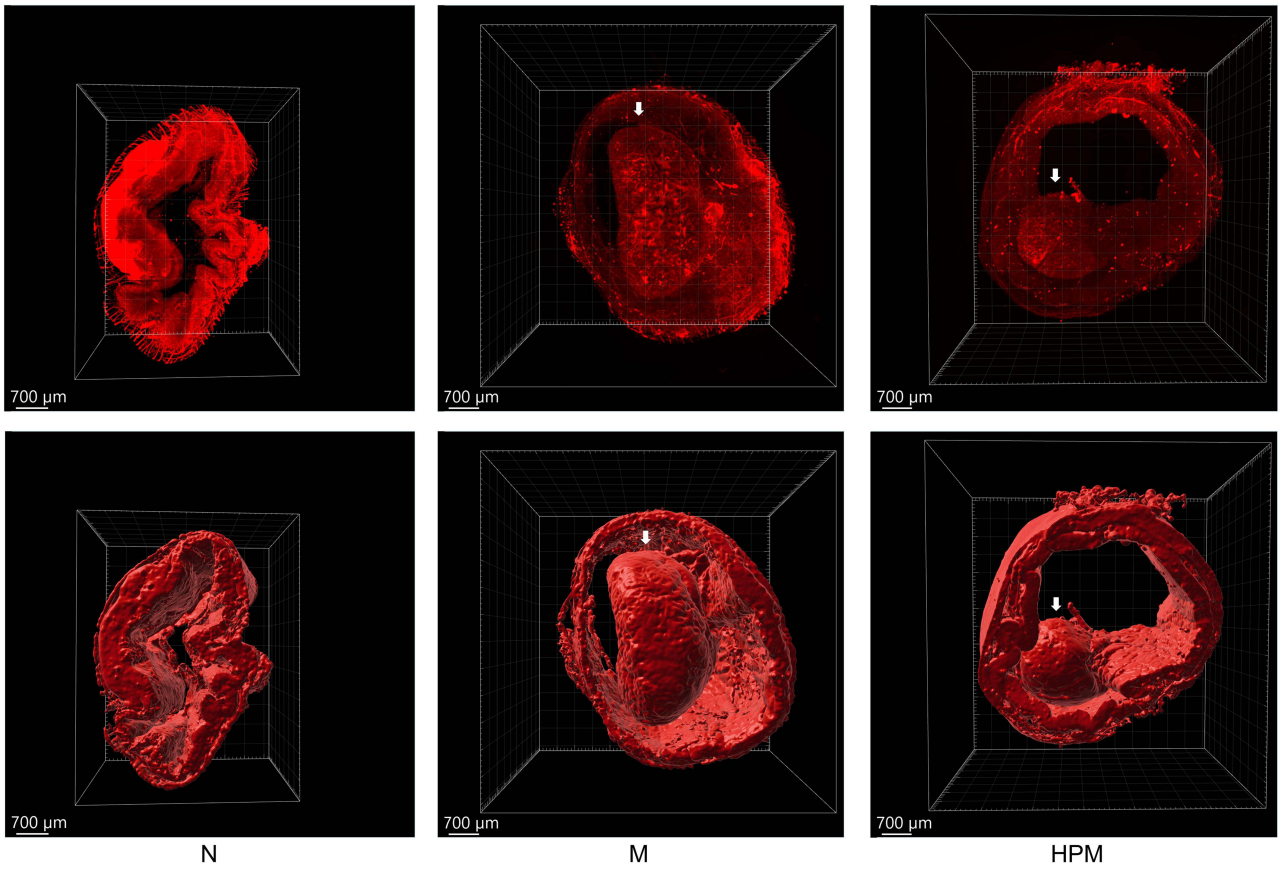

Figure 6 3D imaging of colon tissues by surface. The top part is the original signal and the bottom part is the surface signal. Scale bar: 700 μm.
Abbreviations: N, normal group; M, model group; HPM, herb-partitioned moxibustion group; 3D, three-dimensional.

of branch points, and vessel branch level in the model group were increased as compared to the normal group ($P < 0.01$, $P < 0.001$, $P < 0.001$), and those in the HPM group were decreased compared to the model group ($P < 0.01$, $P < 0.001$, $P < 0.01$; Figure 7A, D and E). The average vessel diameter in the model group showed decreased compared to the normal group ($P < 0.05$), whereas there was no significant difference between the HPM group and the model group ($P > 0.05$; Figure 7B). The average vessel length in the model group was decreased compared to the normal group ($P < 0.01$), and those in the HPM group had an increasing trend, but the difference was not statistically significant compared with the model group ($P > 0.05$; Figure 7C).

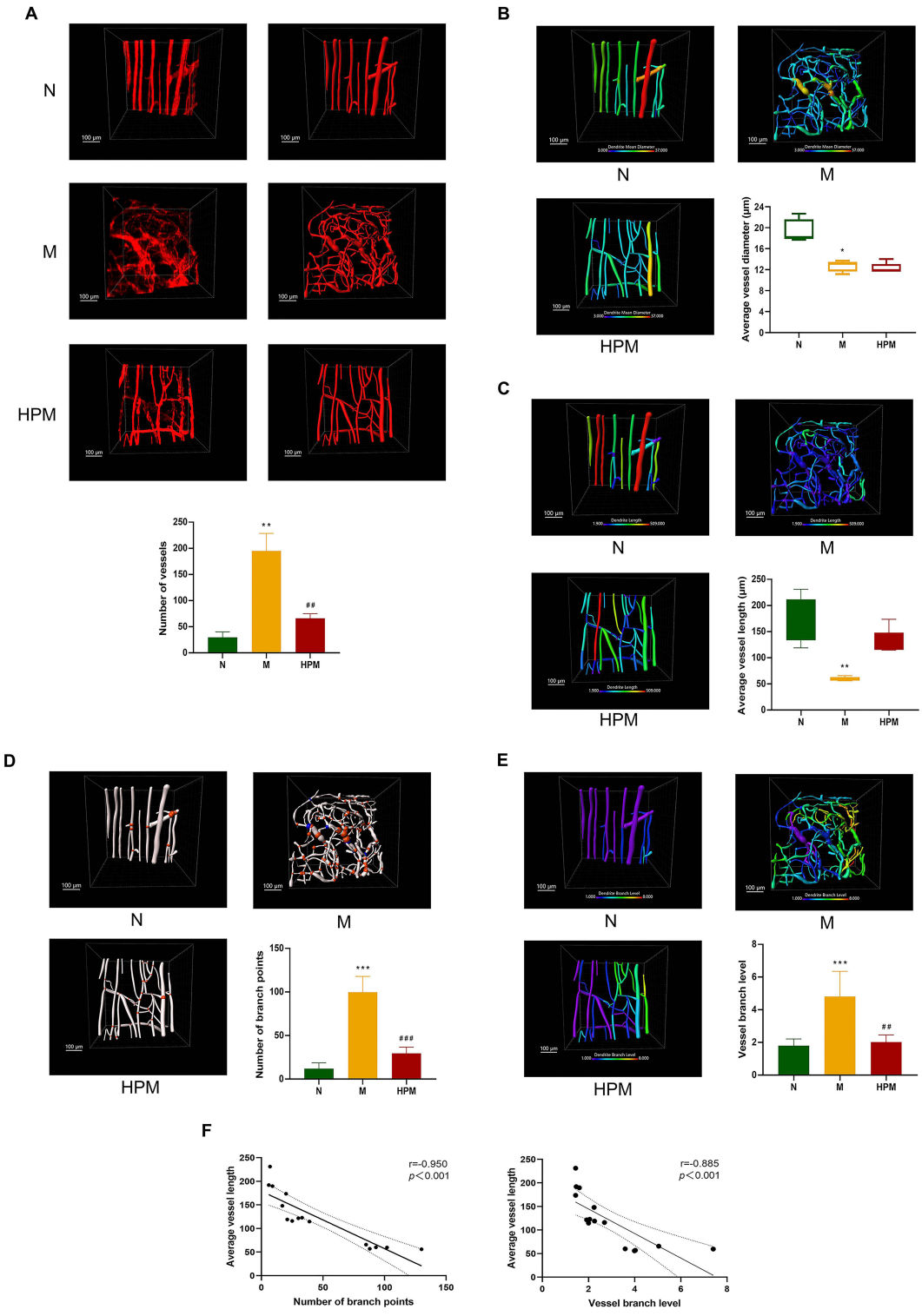

Figure 7 The effect of HPM on 3D vascular architecture in CAC rats. (**A**) Representative 3D images of number of vessels. The left side is the original signal and the right side is the filament signal. (**B**) Representative 3D images of average vessel diameter. (**C**) Representative 3D images of average vessel length. (**D**) Representative 3D images of number of branch points (blue spheres represent four branches, and Orange spheres represent three or two branches). (**E**) Representative 3D images of vessel branch level. (**F**) Association of the number of branch points and vessel branch level with the average vessel length. Scale bar: 100 μm. Statistical significance was determined by One-way ANOVA or Kruskal–Wallis test (n=5); Spearman correlation analysis was calculated for the comparison between the number of branch points, vessel branch level data and the average vessel length data (n=5). $^{*}P < 0.05$, $^{**}P < 0.01$, $^{***}P < 0.001$ (M vs N); $^{\#\#}P < 0.01$, $^{\#\#\#}P < 0.001$ (HPM vs M).

Abbreviations: N, normal group; M, model group; HPM, herb-partitioned moxibustion group; 3D, three-dimensional; CAC, colitis-associated cancer; one-way ANOVA, one-way analysis of variance.

https://doi.org/10.2147/JIR.S518214

To investigate the potential association between the average vascular length and vessel branch characteristics, we further conducted correlation analyses between the vessel branch characteristics (the number of branch points, and vessel branch level) and average vessel length. Quantitative analysis revealed strong inverse correlations, with Spearman's rank coefficients of r =−0.950 for the number of branch points and average vessel length, and r=−0.885 for the vessel branch level and average vessel length. Therefore, both the vessel branch points and vessel branch level were negatively correlated with the average vessel length ($P < 0.001$, $P < 0.001$; Figure 7F).

Discussion

Through our sustained investigation into HPM for IBD, we have identified that HPM as a viable complementary and alternative therapeutic approach had certain advantages and effects in treating IBD.[24,25,27,40,41] HPM is a type of moxibustion, which moxa cones are burned to warm up herb cakes to stimulate acupoints. In recent years, we have explored whether HPM has a role in CAC. In this study, we found that HPM showed significant advantages in reducing tumor size, which is similar to our previous researches.[31,33]

Tumor angiogenesis is the process of the formation of new blood vessels in the tumor to obtain sufficient oxygen and nutrients during tumor growth. The formation of neovasculature in tumors not only provides nutritional support for the sustained growth of tumors, but also is the pathway for the metastasis of tumor cells, which play important roles in both tumor growth and metastasis.[42,43]

The angiogenesis status in neoplastic tissues was assessed through MVD quantification by CD34 immunohistochemistry. In this study, the results indicated that the MVD increased in the model group and decreased in the HPM group. These findings revealed that HPM could reverse the elevated MVD in CAC. VEGF, one of the most important growth factors in promoting angiogenesis, primarily stimulates vascular endothelial cell proliferation and mediates lumen formation. Relevant studies have shown that VEGF expression is significantly elevated in patients with colon cancer.[44,45] Our results also indicated a significant increase of VEGF expression in the model group, HPM attenuated its expression. Meanwhile, the enhancement of the glycolytic pathway in tumor tissues, the degeneration of mitochondrial function and the rapid proliferation of tumor cells result in an anoxic environment.[46] The glycolytic pathway activates the production of ROS.[47] The excessive production of ROS is strongly implicated in the pathological progression from ulcerative colitis to CRC.[48] In our study, we observed HPM can reduce ROS levels, consistent with the findings of Wang X reported that HPM decreased ROS content in CAC mice.[49] ROS generated at mitochondrial complex III stabilizes HIF-1α during hypoxia.[50] The accumulation of HIF-1α activates VEGF and its receptor, thereby increasing the vascular permeability and promoting the formation of nodular vascular buds by vascular endothelial cells.[7,51] In this study, it was found that the expressions of HIF-1α, VEGFA, and VEGFR1 were increased after modeling, accompanied by a decline in HPM group. CAC is a typical model of the pathological process of colitis-induced carcinoma. To elucidate whether HPM inhibition of angiogenesis was linked to inflammatory responses, we quantified key pro-inflammatory cytokines (IL-6, IL-1β, and TNF-α). Our findings revealed that HPM could inhibit the expression of IL-6, IL-1β, and TNF-α. Study found that VEGF was mediated by the proinflammatory cytokine IL-6, which has been shown to be a strong promoter of tumor growth in CAC.[52] Furthermore, both IL-1β and TNF-α exhibited synergistic upregulation with VEGF expression in CAC.[53,54] Therefore, our study suggests a potential inflammatory-angiogenic coupling mechanism that may be targeted by HPM, which needs to be further studied in the future.

With the continuous development and optimization of big data acquisition, processing systems and computer reconstruction technologies, tissue and organ imaging has developed from traditional two-dimensional tissue sections to three-dimensional imaging applications.[55] Emerging tissue clearing techniques have been able to reconstruct complex network structures of large tissues or individual organs, enabling the study of 3D vascular structures at the macroscopic level and fully reflecting subtle changes in the structure of body tissues and organs.

In recent years, tissue optical cleaning techniques have been developed by introducing various chemical agents and tools to reduce scattering and improve the depth of light penetration.[56,57] Numerous tissue-clearing methodologies have been established, with common hydrophilic cleaning methods including clear, unobstructed brain/body imaging cocktails and computational analysis (CUBIC), scale method with sorbitol (ScaleS), and clearT. There are also many organic hydrophobic cleaning methods such as three-dimensional imaging of solvent-cleared organs (3DISCO), immunolabeling-

enabled DISCO (iDISCO), FDISCO, and fluorescence-enabled clearing with benzyl alcohol/benzyl benzoate (FluoClearBABB).[58] The third type of clearing method includes hydrogel-based clearing methods such as clear lipid-exchanged acrylamide-hybridized rigid imaging/immunostaining/in situ-hybridization-compatible tissue-hydrogel (CLARITY), and system-wide control of interaction time and kinetics of chemicals (SWITCH). Hydrophilic cleaning methods can better retain protein-based fluorescence, and organic hydrophobic cleaning methods can provide good clearance speed.[59]

In accordance with the regulatory effects of HPM on the MVD and vascular-related factors, we further used tissue transparency and 3D imaging technology to observe the structure of blood vessels to determine whether HPM affects on the vascular structure of CAC. In this study, an advanced optical clearing method FDISCO, based on 3DISCO, was used to observe the vascular architecture. FDISCO overcomes the shortcomings of 3DISCO, which involves rapid internal fluorescence quenching, and is often used in the presentation of vascular structures.[58] FDISCO has the advantages of rapid processing time, high level of fluorescence preservation, and strong tissue removal ability.[60] Therefore, we used the FDISCO tissue clearing technique to make the tissues transparent, and the 3D imaging to observe the vascular architecture. Intuitive quantitative research could reveal the rule of the blood supply of colon tumor, and describe and estimate the colon tumor blood supply from another perspective.

First, primary analysis utilizing the surface function in Imaris revealed the size of colon tumors in the HPM group was reduced compared to the model group. The colonic vasculature was subsequently intercepted by "Crop" module within the Imaris software, and the parts of the blood vessels were enlarged. Through the original signal and the filament signal, we observed that the colonic blood vessels in the model group exhibited an increased number of colonic vascular branches with disorganized morphology and a reticular distribution pattern compared to the normal group. The HPM group showed a reduction in branched vessels, which were predominantly arranged in a linear configuration compared to the model group. The findings of this study were consistent with previous research indicating that tumor vascular structures are disordered, with abnormal structures of blood vessels and increased abnormal branching.[61,62]

Then, we further statistically analyzed the number of vessels, average vessel diameter, average vessel length, number of branch points, and vessel branch level. Compared with the normal group, the number of vessels in the model group increased, indicating increased blood supply in CAC. HPM played an inhibitory effect on blood supply. These findings are consistent with the results of the MVD and angiogenesis-related cytokine in this study. Our study revealed that compared to the normal group, the model group exhibited a significant increase in both the number of branch points and vessel branch level, while marked reductions in average vessel diameter and length. Meanwhile, both vessel branch point and vessel branch level demonstrated a negative correlation with average vessel length, suggesting that the more vessel branches, the shorter vessel length. These findings are similar to Less JR reported a pattern in the vascular architecture of mammary carcinoma where longer blood vessels have fewer branches.[63] In tumors, blood vessel formation and development occur in a poorly regulated, chaotic manner. In this context, the concept of "vascular normalization" has been established.[64] Research has shown that anti-angiogenic therapy could "normalize" the vascular architecture of tumor, thereby improving their pathological condition and increasing their sensitivity to chemoradiotherapy.[65] We found that HPM played a role in reducing blood vessel branches and had a tendency to make blood vessels longer, but it had no obvious regulatory effect on the average vessel diameter. This may provide insights into the combined application of HPM and anti-angiogenic agents in CAC treatment, particularly molecular-targeted drugs against VEGF/VEGFR pathways such as bevacizumab or regorafenib.

This study represents a preliminary exploration into the effects of HPM on the vasculature of CAC. Several limitations should be acknowledged in this study, primarily the relatively small sample size, the reliance on a single animal model, and lack of dose–response characterization of HPM, which may affect the generalizability of the findings. Future research can be built upon these findings to conduct more deeper, larger sample size studies in conjunction with chemotherapy, radiotherapy or angiogenesis inhibitors (such as VEGF inhibitors).

Conclusion

In summary, we found that HPM may play a role in reducing the blood supply to tumors and normalizing the chaotic tumor vascular system by reducing the formation of branch blood vessels in a CAC model. Our findings may offer

a promising new avenue for the clinical treatment of CAC. However, this study has certain limitations, including a small sample size and the use of a single animal model. We will further study whether HPM can be used as a complementary therapy for chemotherapy, radiotherapy, or anti-angiogenic agents to improve their efficacies in the future, thereby providing novel perspectives for developing combined therapeutic strategies in clinical management of CAC.

Abbreviations

3D, Three-dimensional; 3DISCO, Three-dimensional imaging of solvent-cleared organs; AOM, Azoxymethane; CAC, Colitis-associated cancer; CD34, Cluster of differentiation 34 antigen; CRC, Colorectal cancer; DSS, Dextran sodium sulphate; ELISA, Enzyme-linked immunosorbent assay; FDISCO, Three-dimensional imaging of solvent-cleared organs with superior fluorescence-preserving capability; HE, Hematoxylin-eosin; HIF-1α, Hypoxia-inducible factor-1 alpha; HPM, Herb-partitioned moxibustion; IBD, Inflammatory bowel disease; IL-1β, Interleukin-1 beta; IL-2, Interleukin-2; IL-6, Interleukin-6; LSD, Least significant difference; MVD, Microvessel density; PECAM-1, Platelet endothelial cell adhesion molecule 1; ROS, Reactive oxygen species; TNF-α, Tumor necrosis factor-alpha; VEGFA, Vascular endothelial growth factor A; VEGFR1, Vascular endothelial growth factor receptor 1.

Data Sharing Statement

The relevant datasets analysed in this study can be obtained by contacting the corresponding author on reasonable request.

Ethics Approval

This study has been approved by the Animal Ethics Committee of Shanghai University of Traditional Chinese Medicine (PZSHUTCM2306050013).

Acknowledgments

For image analyses, we thank Dr. Yi Feng lab of Department of Integrative Medicine and Neurobiology, School of Basic Medical Sciences, Fudan University for tissue clearing process, light-sheet microscope imaging, as well as core facility for large-scale tissue clearing and data analysis.

Author Contributions

All the authors made an important contribution to the work reported, whether that was in the study design, conception, execution, acquisition of data, analysis and interpretation, or in all these areas: taking part in drafting, critically reviewing or revising the article. All the authors gave final approval of the version to be published and agreed on the journal to which the article has been submitted as well as agreed to be accountable for all aspects of the work.

Funding

This project was supported by National Natural Science Foundation of China (No. 82205261).

Disclosure

The authors report no conflicts of interest in this work.

References

1. Dzhalilova D, Zolotova N, Fokichev N, Makarova O. Murine models of colorectal cancer: the azoxymethane (AOM)/dextran sulfate sodium (DSS) model of colitis-associated cancer. *PeerJ*. 2023;11:e16159. doi:10.7717/peerj.16159
2. Reznicek E, Arfeen M, Shen B, Ghouri YA. Colorectal dysplasia and cancer surveillance in ulcerative colitis. *Diseases*. 2021;9(4):86. doi:10.3390/diseases9040086
3. Beaugerie L, Itzkowitz SH. Cancers complicating inflammatory bowel disease. *N Engl J Med*. 2015;372(15):1441–1452. doi:10.1056/NEJMra1403718
4. Ou B, Zhao J, Guan S, Lu A. Survival of colorectal cancer in patients with or without inflammatory bowel disease: a meta-analysis. *Dig Dis Sci*. 2016;61(3):881–889. doi:10.1007/s10620-015-3940-1

5. Patel SA, Nilsson MB, Le X, Cascone T, Jain RK, Heymach JV. Molecular mechanisms and future implications of VEGF/VEGFR in cancer therapy. *Clin Cancer Res*. 2023;29(1):30–39. doi:10.1158/1078-0432.CCR-22-1366
6. Shi S, Ou X, Liu C, Wen H, Ke J. Research progress of HIF-1a on immunotherapy outcomes in immune vascular microenvironment. *Front Immunol*. 2025;16:1549276. doi:10.3389/fimmu.2025.1549276
7. Lu S, Cai Y, Kang T, Zhu C, Feng Z, Chen S. Arsenic sulfide inhibits hepatocellular carcinoma metastasis by suppressing the HIF-1α/VEGF pathway. *Front Biosci*. 2023;28(7):152. doi:10.31083/j.fbl2807152
8. Schroedl C, McClintock DS, Budinger GR, Chandel NS. Hypoxic but not anoxic stabilization of HIF-1alpha requires mitochondrial reactive oxygen species. *Am J Physiol Lung Cell Mol Physiol*. 2002;283(5):L922–L931. doi:10.1152/ajplung.00014.2002
9. Ludwig N, Whiteside TL. Potential roles of tumor-derived exosomes in angiogenesis. *Expert Opin Ther Targets*. 2018;22(5):409–417. doi:10.1080/14728222.2018.1464141
10. Waldner MJ, Wirtz S, Jefremow A, et al. VEGF receptor signaling links inflammation and tumorigenesis in colitis-associated cancer. *J Exp Med*. 2010;207(13):2855–2868. doi:10.1084/jem.20100438
11. Xie LS, Huan T, Yang JL, Wu J, Zhao P. The effect of Shendan Sanjie capsule on angiogenesis in mice with colitis associated cancer and mechanism. *Chin J Oncol*. 2021;43(11):1170–1176. doi:10.3760/cma.j.cn112152-20210318-00240
12. Liu X, Liu Y, Liu Z, et al. CircMYH9 drives colorectal cancer growth by regulating serine metabolism and redox homeostasis in a p53-dependent manner. *Mol Cancer*. 2021;20(1):114. doi:10.1186/s12943-021-01412-9
13. Brunelle JK, Bell EL, Quesada NM, et al. Oxygen sensing requires mitochondrial ROS but not oxidative phosphorylation. *Cell Metab*. 2005;1(6):409–414. doi:10.1016/j.cmet.2005.05.002
14. Yu T, Qi Y, Gong H, Luo Q, Zhu D. Optical clearing for multiscale biological tissues. *J Biophotonics*. 2018;11(2). doi:10.1002/jbio.201700187
15. Zhou G, Wu H, Lin J, Lin R, Feng B, Liu Z. TRIM21 is decreased in colitis-associated cancer and negatively regulates epithelial carcinogenesis. *Inflamm Bowel Dis*. 2021;27(4):458–468. doi:10.1093/ibd/izaa229
16. Sun L, He Z, Ke J, et al. PAF receptor antagonist Ginkgolide B inhibits tumourigenesis and angiogenesis in colitis-associated cancer. *Int J Clin Exp Pathol*. 2015;8(1):432–440.
17. Pagano E, Elias JE, Schneditz G, et al. Activation of the GPR35 pathway drives angiogenesis in the tumour microenvironment. *Gut*. 2022;71(3):509–520. doi:10.1136/gutjnl-2020-323363
18. Miyamoto R, Nagai K, Kemmochi A, Inagawa S, Yamamoto M. Three-dimensional reconstruction of the vascular arrangement including the inferior mesenteric artery and left colic artery in laparoscope-assisted colorectal surgery. *Surg Endosc*. 2016;30(10):4400–4404. doi:10.1007/s00464-016-4758-4
19. Ding Y, Zhao B, Niu W, et al. Assessing anatomical variations of the inferior mesenteric artery via three-dimensional CT angiography and laparoscopic colorectal surgery: a retrospective observational study. *Sci Rep*. 2024;14(1):6985. doi:10.1038/s41598-024-57661-3
20. Murono K, Kawai K, Ishihara S, et al. Evaluation of the vascular anatomy of the right-sided colon using three-dimensional computed tomography angiography: a single-center study of 536 patients and a review of the literature. *Int J Colorectal Dis*. 2016;31(9):1633–1638. doi:10.1007/s00384-016-2627-1
21. Willard CD, Kjaestad E, Stimec BV, Edwin B, Ignjatovic D; RCC Study Group. Preoperative anatomical road mapping reduces variability of operating time, estimated blood loss, and lymph node yield in right colectomy with extended D3 mesenterectomy for cancer. *Int J Colorectal Dis*. 2019;34(1):151–160. doi:10.1007/s00384-018-3177-5
22. Zhai CT, Jia Y. Analysis of clinical application of different moxibustion methods in intervention of cancer-related diseases based on modern literature. *J Basic Chin Med*. 2019;25(12):1719–1721, 1736. doi:10.19945/j.cnki.issn.1006-3250.2019.12.026
23. Qi Q, Im H, Li KS, et al. Influence of herb-partitioned moxibustion at Qihai (CV6) and bilateral Tianshu (ST25) and Shangjuxu (ST37) acupoints on toll-like receptors 4 signaling pathways in patients with ulcerative coliti. *J Tradit Chin Med*. 2021;41(3):479–485. doi:10.19852/j.cnki.jtcm.20210310.001
24. Im HY, Wang WJ, Qi Q, et al. Clinical efficacy of moxibustion for ulcerative colitis and its influence on vitamin D receptor. *J Acupunct Tuina Sci*. 2023;21(1):40–50. doi:10.1007/s11726-023-1357-5
25. Bao CH, Zhao JM, Liu HR, et al. Randomized controlled trial: moxibustion and acupuncture for the treatment of Crohn's disease. *World J Gastroenterol*. 2014;20(31):11000–11011. doi:10.3748/wjg.v20.i31.11000
26. Bao CH, Wu LY, Wu HG, et al. Moxibustion inhibits apoptosis and tumor necrosis factor-alpha/tumor necrosis factor receptor 1 in the colonic epithelium of Crohn's disease model rats. *Dig Dis Sci*. 2012;57(9):2286–2295. doi:10.1007/s10620-012-2161-0
27. Zhou EH, Liu HR, Wu HG, et al. Down-regulation of protein and mRNA expression of IL-8 and ICAM-1 in colon tissue of ulcerative colitis patients by partition-herb moxibustion. *Dig Dis Sci*. 2009;54:2198–2206. doi:10.1007/s10620-008-0620-4
28. Gu XY, Gao ZQ, Zhang ZJ, Huang ZM, Xie XH. Influence of warming needling technique on gastrointestinal reaction after hyperthermic intraperitoneal chemotherapy in patients with postoperation of colon cancer. *Acupunt Res*. 2020;45(4):315–319. doi:10.13702/j.1000-0607.190385
29. Zhang T, Kang XD. Research progress of traditional Chinese and western medicine in the treatment of colon cancer. *Systems Med*. 2019;4(23):192–194. doi:10.19368/j.cnki.2096-1782.2019.23.192
30. Lu Y, Gu ME, Ding BY, et al. Research on the effects of moxibustion on P2X7 receptor and Wnt/β-catenin signaling pathway in colitis-associated cancer rats. *Shanghai J Acu-Mox*. 2020;39(6):758–765. doi:10.13460/j.issn.1005-0957.2020.13.1042
31. Yao CJ, Qin Q, Zhao JM, et al. Study on the circRNA expression profile related to colonic tumor proliferation regulated by acupuncture-moxibustion in colitis-associated colorectal cancer rats. *Shanghai J Acu-Mox*. 2024;43(11):1257–1268. doi:10.13460/j.issn.1005-0957.2023.13.3012
32. Xu HX, Wang YR, Xu J, et al. Study on the mechanism of herb cake-partitioned moxibustion inhibiting tumor growth in colitis-associated colorectal cancer based on KDM4D receptor. *J Acupunct Tuina Sci*. 2024;22(1):1–11. doi:10.1007/s11726-024-1418-4
33. Lin YY, Wang D, Wu HG, et al. Effects of moxibustion on the P2X7R/STAT3/VEGF pathway in rats with colitis-associated colon cancer. *J Acupunct Tuina Sci*. 2021;19(2):83–94. doi:10.1007/s11726-021-1230-3
34. Modesto R, Estarreja J, Silva I, Rocha J, Pinto R, Mateus V. Chemically Induced colitis-associated cancer models in rodents for pharmacological modulation: a systematic review. *J Clin Med*. 2022;11(10):2739. doi:10.3390/jcm11102739
35. Josa V, Ferenczi S, Szalai R, et al. Thrombocytosis and effects of IL-6 knock-out in a colitis-associated cancer model. *Int J Mol Sci*. 2020;21(17):6218. doi:10.3390/ijms21176218

36. Arimura Y, Nagaishi K, Hosokawa M. Dynamics of claudins expression in colitis and colitis-associated cancer in rat. *Methods Mol Biol*. 2011;762:409–425. doi:10.1007/978-1-61779-185-729
37. Tajasuwan L, Kettawan A, Rungruang T, et al. Inhibitory effect of dietary defatted rice bran in an AOM/DSS-induced colitis-associated colorectal cancer experimental animal model. *Foods*. 2022;11(21):3488. doi:10.3390/foods11213488
38. Tajasuwan L, Kettawan A, Rungruang T, Wunjuntuk K, Prombutara P. Role of Dietary defatted rice bran in the modulation of gut microbiota in AOM/DSS-induced colitis-associated colorectal cancer rat model. *Nutrients*. 2023;15(6):1528. doi:10.3390/nu15061528
39. Shi Y, Bao CH, Wu HG, et al. Effects of herbs-partitioned moxibustion on the expressions of intestinal mucosa TNF-α, TNFR1, TNFR2 and apoptosis of intestinal epithelial cells in Crohn's disease patients. *Shanghai J Tradit Chin Med*. 2011;45:46–50. doi:10.16305/j.1007-1334.2011.01.026
40. Wang X, Liu Y, Dong H, et al. Herb-partitioned moxibustion regulates the TLR2/NF-κB signaling pathway in a rat model of ulcerative colitis. *Evid Based Complement Alternat Med*. 2015;2015:949065. doi:10.1155/2015/949065
41. Ji R, Wang A, Shang H, et al. Herb-partitioned moxibustion upregulated the expression of colonic epithelial tight junction-related proteins in Crohn's disease model rats. *Chin Med*. 2016;11:20. doi:10.1186/s13020-016-0090-0
42. Shimizu K, Oku N. Cancer anti-angiogenic therapy. *Biol Pharm Bull*. 2004;27(5):599–605. doi:10.1248/bpb.27.599
43. Tang XH. The current status and progress of basic research on the anti-tumor angiogenesis of traditional Chinese medicine. *Jilin J Tradit Chin Med*. 2010;30(9):825–828. doi:10.13463/j.cnki.jlzyy.2010.09.035
44. Abdulla MH, Shaik AS, Vaali-Mohammed MA, et al. Expression of VEGF, EGF and HGF in early- and late-stage colorectal cancer. *Mol Clin Oncol*. 2021;15(6):251. doi:10.3892/mco.2021.2413
45. Ghonbalani ZN, Shahmohamadnejad S, Pasalar P, Khalili E. Hypermethylated miR-424 in colorectal cancer subsequently upregulates VEGF. *J Gastrointest Cancer*. 2022;53(2):380–386. doi:10.1007/s12029-021-00614-0
46. Liberti MV, Locasale JW. The Warburg effect: how does it benefit cancer cells? *Trends Biochem Sci*. 2016;41(3):211–218. doi:10.1016/j.tibs.2015.12.001
47. Ye XY, Niu XM, Gu LP, et al. Desuccinylation of pyruvate kinase M2 by SIRT5 contributes to antioxidant response and tumor growth. *Oncotarget*. 2017;8(4):6984–6993. doi:10.18632/oncotarget.14346
48. Irrazabal T, Thakur BK, Croitoru K, Martin A. Preventing colitis-associated colon cancer with antioxidants: a systematic review. *Cell Mol Gastroenterol Hepatol*. 2021;11(4):1177–1197. doi:10.1016/j.jcmgh.2020.12.013
49. Wang X, Ji H, Yang Y, et al. Moxibustion regulates the BRG1/Nrf2/HO-1 pathway by inhibiting microRNA-222-3p to prevent oxidative stress in intestinal epithelial cells in ulcerative colitis and colitis-associated colorectal cancer. *J Immunol Res*. 2024;2024:8273732. doi:10.1155/2024/8273732
50. Chandel NS, McClintock DS, Feliciano CE, et al. Reactive oxygen species generated at mitochondrial complex III stabilize hypoxia-inducible factor-1alpha during hypoxia: a mechanism of O_2 sensing. *J Biol Chem*. 2000;275(33):25130–25138. doi:10.1074/jbc.M001914200
51. Hansen TF, Spindler KL, Lorentzen KA, et al. The importance of −460 C/T and +405 G/C single nucleotide polymorphisms to the function of vascular endothelial growth factor A in colorectal cancer. *J Cancer Res Clin Oncol*. 2010;136(5):751–758. doi:10.1007/s00432-009-0714-1
52. Becker C, Fantini MC, Schramm C, et al. TGF-beta suppresses tumor progression in colon cancer by inhibition of IL-6 trans-signaling. *Immunity*. 2004;21(4):491–501. doi:10.1016/j.immuni.2004.07.020
53. Hardbower DM, Coburn LA, Asim M, et al. EGFR-mediated macrophage activation promotes colitis-associated tumorigenesis. *Oncogene*. 2017;36(27):3807–3819. doi:10.1038/onc.2017.23
54. Koh SJ, Kim JW, Kim BG, Lee KL, Kim DW, Kim JS. Matricellular protein periostin promotes colitis-associated colon tumorigenesis in mice. *Carcinogenesis*. 2019;40(1):102–111. doi:10.1093/carcin/bgy120
55. Li YZ, Shao ZH, Li SG. Application of clearing methods on tissues in the three-dimensional imaging research. *Acta Anatomica Sinica*. 2018;49(3):400–405. doi:10.16098/j.issn.0529-1356.2018.03.022
56. Silvestri L, Costantini I, Sacconi L, Pavone FS. Clearing of fixed tissue: a review from a microscopist's perspective. *J Biomed Opt*. 2016;21(8):081205. doi:10.1117/1.Jbo.21.8.081205
57. Susaki EA, Ueda HR. Whole-body and whole-organ clearing and imaging techniques with single-cell resolution: toward organism-level systems biology in mammals. *Cell Chem Biol*. 2016;23(1):137–157. doi:10.1016/j.chembiol.2015.11.009
58. Wan P, Li YS, Zhu JT, et al. FDISCO+: a clearing method for robust fluorescence preservation of cleared samples. *Neurophotonics*. 2021;8(3):035007. doi:10.1117/1.NPh.8.3.035007
59. Wan P, Zhu JT, Xu JY, Li YS, Yu TT, Zhu D. Evaluation of seven optical clearing methods in mouse brain. *Neurophotonics*. 2018;5(3):035007. doi:10.1117/1.NPh.5.3.035007
60. Qi YS, Yu TT, Xu JY, et al. FDISCO: advanced solvent-based clearing method for imaging whole organs. *Sci Adv*. 2019;5(1):eaau8355. doi:10.1126/sciadv.aau8355
61. Demené C, Payen T, Dizeux A, et al. 3-D longitudinal imaging of tumor angiogenesis in mice in vivo using ultrafast Doppler tomography. *Ultrasound Med Biol*. 2019;45(5):1284–1296. doi:10.1016/j.ultrasmedbio.2018.12.010
62. Hoyt K, Umphrey H, Lockhart M, Robbin M, Forero-Torres A. Ultrasound imaging of breast tumor perfusion and neovascular morphology. *Ultrasound Med Biol*. 2015;41(9):2292–2302. doi:10.1016/j.ultrasmedbio.2015.04.016
63. Less JR, Skalak TC, Sevick EM, Jain RK. Microvascular architecture in a mammary carcinoma: branching patterns and vessel dimensions. *Cancer Res*. 1991;51(1):265–273.
64. Goel S, Duda DG, Xu L, et al. Normalization of the vasculature for treatment of cancer and other diseases. *Physiol Rev*. 2011;91(3):1071–1121. doi:10.1152/physrev.00038.2010
65. Ascheid D, Baumann M, Funke C, et al. Image-based modeling of vascular organization to evaluate anti-angiogenic therapy. *Biol Direct*. 2023;18(1):10. doi:10.1186/s13062-023-00365-x

Journal of Inflammation Research

Dovepress
Taylor & Francis Group

Publish your work in this journal

The Journal of Inflammation Research is an international, peer-reviewed open-access journal that welcomes laboratory and clinical findings on the molecular basis, cell biology and pharmacology of inflammation including original research, reviews, symposium reports, hypothesis formation and commentaries on: acute/chronic inflammation; mediators of inflammation; cellular processes; molecular mechanisms; pharmacology and novel anti-inflammatory drugs; clinical conditions involving inflammation. The manuscript management system is completely online and includes a very quick and fair peer-review system. Visit http://www.dovepress.com/testimonials.php to read real quotes from published authors.

Submit your manuscript here: https://www.dovepress.com/journal-of-inflammation-research-journal